

The Effect of the Lanthanide Ion-Type in LnFeO_3 on the Catalytic Activity for the Hydrogen Evolution in Acidic Medium

Nada F. Atta*, Ahmed Galal, Shima M. Ali

Department of Chemistry, Faculty of Science, Cairo University, 12613 Giza, Egypt

*E-mail: nada_fahl@yahoo.com

Received: 18 November 2013 / Accepted: 5 January 2014 / Published: 2 February 2014

LnFeO_3 (Ln = La, Nd, Sm and Gd) were prepared by microwave-assistant citrate method and characterized by XRD and SEM. The electrocatalytic activity toward hydrogen evolution reaction (HER) was investigated by Tafel polarization and impedance measurements. The order of the electrocatalytic activity was $\text{NdFeO}_3 > \text{LaFeO}_3 > \text{SmFeO}_3 > \text{GdFeO}_3$, according to the calculated values of the activation energy. The reaction order and the reaction mechanism for all the prepared perovskites were identified. In addition, the effect of the partial substitution at the Lanthanide-site in $\text{La}_{1-y}\text{Sm}_y\text{FeO}_3$ was also studied.

Keywords: Perovskites; Microwave Synthesis; Catalyst; Hydrogen Evolution; Impedance; Tafel.

1. INTRODUCTION

The hydrogen evolution reaction (HER) is an attractive reaction that illustrates the importance of research in the field of renewable energy. There is a significant technological interest in this reaction due to its important role in electrodeposition and corrosion of metals in acids, in storage of energy via hydrogen production, and as the microscopic reverse of the hydrogen oxidation reaction in low-temperature fuel cells [1-3]. The electrocatalysis in the HER is one of the most important subjects in the field of electrochemistry. Three properties play an important role in selecting catalytically active materials for hydrogen evolution: (a) an actual intrinsic electrocatalytic effect of the material, (b) a large active surface area per unit volume ratio, both of which are directly related to the overpotential used to operate the electrolyzer at significant current densities, and (c) catalyst stability [4]. Thus, from an electrochemical point of view, the problem to be tackled in order to decrease the cost of electrolytic hydrogen is the reduction of overpotentials. The desired decrease in overpotential

can be achieved by choosing highly catalytically active electrode materials, or by increasing the active surface area of the electrode.

The microwave irradiation process (MIP), which is one of the novel processes evolved from microwave sintering, was widely applied in inorganic/organic synthesis, food drying, microwave-induced catalysis and plasma chemistry. With its rapid development in recent decades, MIP has obtained a growing interest, especially in materials synthesis research. The advantages of MIP have been summarized as below: (i) rapid reaction velocity; (ii) uniform heating; (iii) clean and energy efficient. During the past years, a lot of perovskites ABO_3 (A: alkaline earth or lanthanide; B: transition element), such as $GaAlO_3$, $LaCrO_3$, etc., have been reported to be synthesized by MIP for their ferroelectricity, superconductivity, high-temperature ionic conductivity, or a variety of magnetic ordering, etc. [5-7]. It was reported that smaller grain size and more rapid lattice diffusion would be formed in microwave route than other wet chemical processes [8], which might enhance the lattice oxygen mobility in catalysis process. However, secondary phases were formed during the perovskite synthesis by MIP [9] and the average particle size obtained was relatively higher than that obtained by other conventional synthesis method such as sol-gel method.

The A-site metal in perovskites not only has a strong effect on the stability of the whole crystal configuration, but also provides the possibility to improve catalyst performance by synergetic interactions with metals on B-site. For this reason, it is necessary to choose suitable metal ions on A-site in this kind of structure. Among the pioneering works [10], lanthanum was preferred for its long-certified promotion effect on thermal stability and activity. However other lanthanide elements showed strong redox property in catalytic systems.

In this work, a series of $LnFeO_3$ ($Ln = La, Nd, Sm$ and Gd) were prepared by the microwave assistant-citrate method. This method combined the advantages of both MIP and citrate-nitrate method. As a single-phase perovskite of uniform particle size distribution, small average particle size (in the nanometer scales) and enhanced catalytic properties can be obtained [11]. The influence of the type of the lanthanide ion on the catalytic activity for HER was studied by Tafel and electrochemical impedance measurements. A complete kinetics study was carried out in which the reaction order, the activation energy and the reaction mechanism were identified. In addition, the effect of the partial substitution at the Lanthanide-site in $La_{1-y}Sm_yFeO_3$ was also studied.

2. MATERIALS AND METHODS

2.1. Chemicals

Lanthanum (III) nitrate hexahydrate (Sigma-Aldrich, puriss. p.a., 99%), Samarium(III) nitrate hexahydrate (Acros-Organics, 99.9%), Neodymium(III) nitrate hexahydrate (Strem Chemicals, 99.9%-Nd, REO), Gadolinium (III) nitrate hexahydrate (Strem Chemicals, 99.9%-Gd, REO), Iron(III) nitrate (Pharma Chem, 99%), Citric acid, Nitric acid, Sulfuric acid, ammonia, (Aldrich), Graphite powder (Sigma-Aldrich, <20 micron, synthetic) and Paraffin oil (Fluka) were used as received without further purification. All solutions were prepared using double distilled water. All measurements were made

in oxygen-free solution, which was achieved by continuous purging of the cell electrolyte with nitrogen gas (99.999% pure).

2.2. Catalyst preparation

Stoichiometric measurements of Ln-nitrate and Ferric-nitrate were weighed, dissolved in distilled water and stirred for 5 min. To this aqueous solution, a sufficient amount of citric acid was added so that the molar ratio of citric acid to total metal ions is 1:1. The solution was stirred well for uniform mixing. Ammonia was added to adjust the pH of the solution at 6. The solution was placed in a conventional microwave oven, with an operating power of 720 W, and the reaction was performed under ambient air for 30 minutes. The microwave was operated in 30-s cycles (20 s on, 10 s off) [11-13]. The precursor complex dehydrated and became more viscous with time producing a dark gel. The gel got ignited giving a voluminous fluffy powder. A ceramic nano-oxide was then obtained by calcinations at temperature = 900°C.

2.3. Electrochemical cell and equipments

A standard three-electrode, one compartment cell was used in all experiments. The counter electrode was a large surface area platinum electrode. The reference electrode was a commercially available saturated silver/silver chloride electrode. The working electrode was a carbon paste electrode (CPE) ($d=0.63\text{cm}$), the unmodified CPE was prepared as follows: 0.125 g of reagent grade graphite powder was taken, washed with acetone, and dried which was then mixed with 45 μL of paraffin oil. To modify the CPE, the graphite powder was mixed with the modifier in a certain composition ratio. Both unmodified and modified carbon pastes were packed into a Teflon holder that had been cut off at the end. Electrical contact to the paste was established via a thin copper rod passed through the Teflon holder. The fresh surfaces were obtained by polishing the electrodes on a clean paper until they showed a smooth and shiny appearance after every measurement.

All electrochemical measurements, the DC polarization and the electro-chemical impedance spectroscopy (EIS), were carried out in 0.1M H_2SO_4 aqueous acid by using a Gamry-750 system and a lock-in-amplifier that are connected to a personal computer.

DC polarization measurements of hydrogen evolution were carried out by first stabilization at open-circuit potential (OCP) until a steady-state OCP value was obtained (usually about 30 min.), then conditioning the electrode at -0.2V for 10 min. and at -0.3V for 5 min. Then a linear polarization measurement was made starting from -0.3V to -0.6V, at a scan rate of $1\text{mV}\cdot\text{s}^{-1}$. The DC polarization measurement was followed by a set of electrochemical impedance spectroscopy measurements at selected overpotentials.

The order of the reaction with respect to H^+ was determined at constant ionic strength of the solution by varying the H_2SO_4 concentration between 0.05 and 0.5M (6 solutions), keeping the ionic strength constant with Na_2SO_4 . Only one DC polarization measurement was taken at each H_2SO_4 concentration by the same procedure mentioned above.

The Scanning electron microscopy analysis was done by using Philips XL30. X-ray diffraction analysis was obtained using Shimadzu XRD-700.

3. RESULTS AND DISCUSSION

3.1. XRD and surface characterization

LnFeO_3 ($\text{Ln} = \text{La}, \text{Nd}, \text{Sm}$ and Gd) were prepared by microwave-assistant citrate method at a microwave operating power of 720 W and a microwave irradiation time of 30 min. All four prepared perovskites, lanthanum ferrite, Neodymium ferrite, Samarium ferrite and Gadolinium ferrite and all had fairly high tolerance factors, which were 0.838, 0.821, 0.814 and 0.807, respectively. Figure 1 shows the XRD of (A) LaFeO_3 , (B) NdFeO_3 , (C) SmFeO_3 and (D) GdFeO_3 prepared by microwave assistant-citrate method. XRD characterization proved that pure perovskite crystals were indeed formed, the major diffraction peaks of the as-synthesized powders were matched with the theoretical ones. The results suggested successful incorporation of Fe^{3+} at the La^{3+} , Nd^{3+} , Sm^{3+} and Gd^{3+} cation sites confirming the formation of the orthorhombic phase of LaFeO_3 , NdFeO_3 , SmFeO_3 and GdFeO_3 .

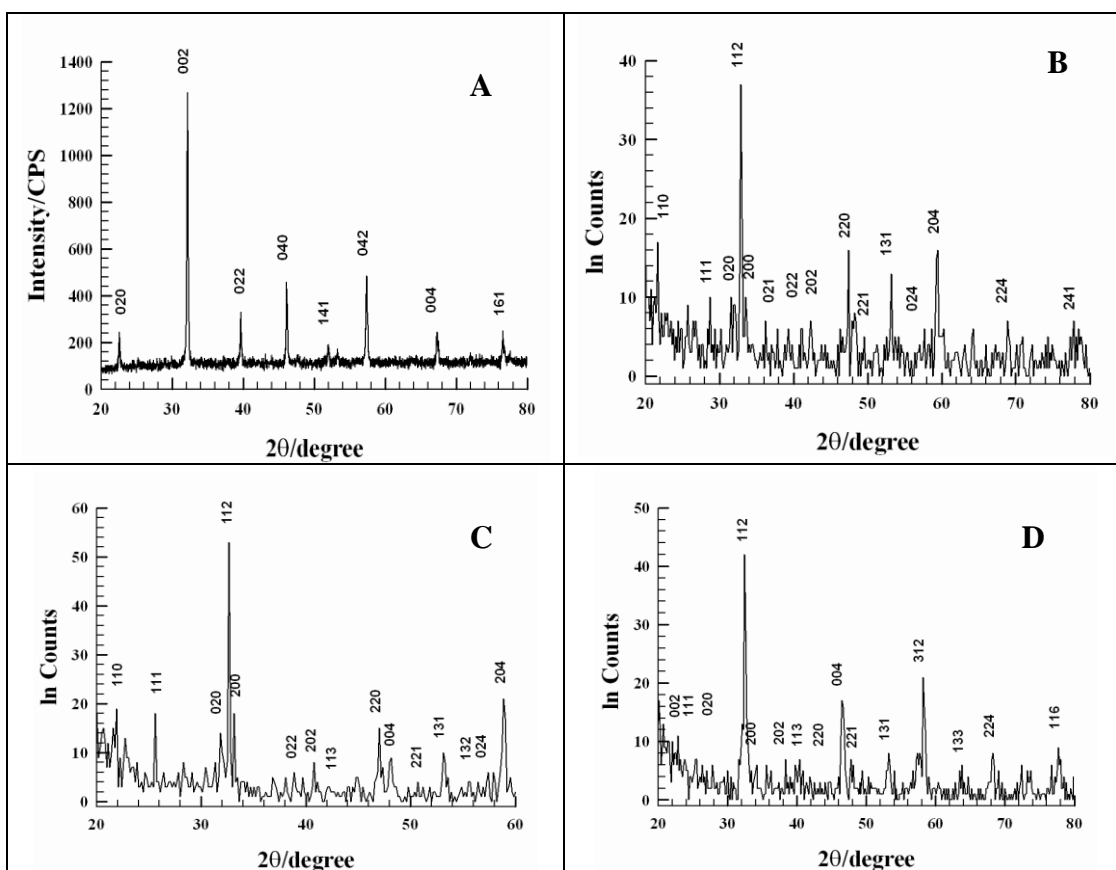


Figure 1. XRD patterns of (A) LaFeO_3 , (B) NdFeO_3 , (C) SmFeO_3 and (D) GdFeO_3 prepared by the microwave-assistant citrate method at 720 W for 30 min. Miller indices (h, l, k) are showed.

Some important structural parameters were calculated from XRD data such as, particle size, lattice parameters, lattice volume and theoretical density [14]. These parameters were calculated and listed in Table 1. A good agreement with those for standards was found. The observed difference in the unit cell volume, V , agrees with that expected from the difference in size volume of the involved rare-earth ions.

The morphology of the prepared perovskites was studied by SEM. Figure 2 shows the SEM images of (A) LaFeO_3 , (B) NdFeO_3 , (C) SmFeO_3 and (D) GdFeO_3 prepared by microwave assistant-citrate method. It can be seen that changing the type of the A-site metal ion did not affect the morphology of the prepared perovskites greatly. All samples were composed of network of grains of bone-like shape. However there was a difference in the degree of porosity and the grain size.

Table 1. Structural parameters, calculated from XRD data, for standard LnFeO_3 ($\text{Ln} = \text{La}, \text{Nd}, \text{Sm}$ and Gd) and those prepared by the microwave-assistant citrate method at 720 W for 30 min.

	Crystal Structure	Average Particle Size/nm	Lattice Parameters \AA	Lattice Volume \AA^3	Theoretical density g/cm^3
Standard LaFeO_3	Orthorhombic		a = 5.556 b = 5.565 c = 7.855	242.86	6.64
LaFeO_3 Sample	Orthorhombic	91.7	a = 5.559 b = 5.579 c = 7.862	243.83	6.63
Standard NdFeO_3	Orthorhombic		a = 5.453 b = 5.584 c = 7.768	236.53	6.97
NdFeO_3 Sample	Orthorhombic	87.9	a = 5.458 b = 5.587 c = 7.750	236.33	6.98
Standard SmFeO_3	Orthorhombic		a = 5.400 b = 5.597 c = 7.711	233.06	7.25
SmFeO_3 Sample	Orthorhombic	100.2	a = 5.404 b = 5.574 c = 7.697	231.85	7.25
Standard GdFeO_3	Orthorhombic		a = 5.349 b = 5.611 c = 7.669	230.17	7.53
GdFeO_3 Sample	Orthorhombic	46.8	a = 5.350 b = 5.565 c = 7.684	228.77	7.54

3.2. Investigation of the catalytic activity toward HER by DC-Tafel linear polarization

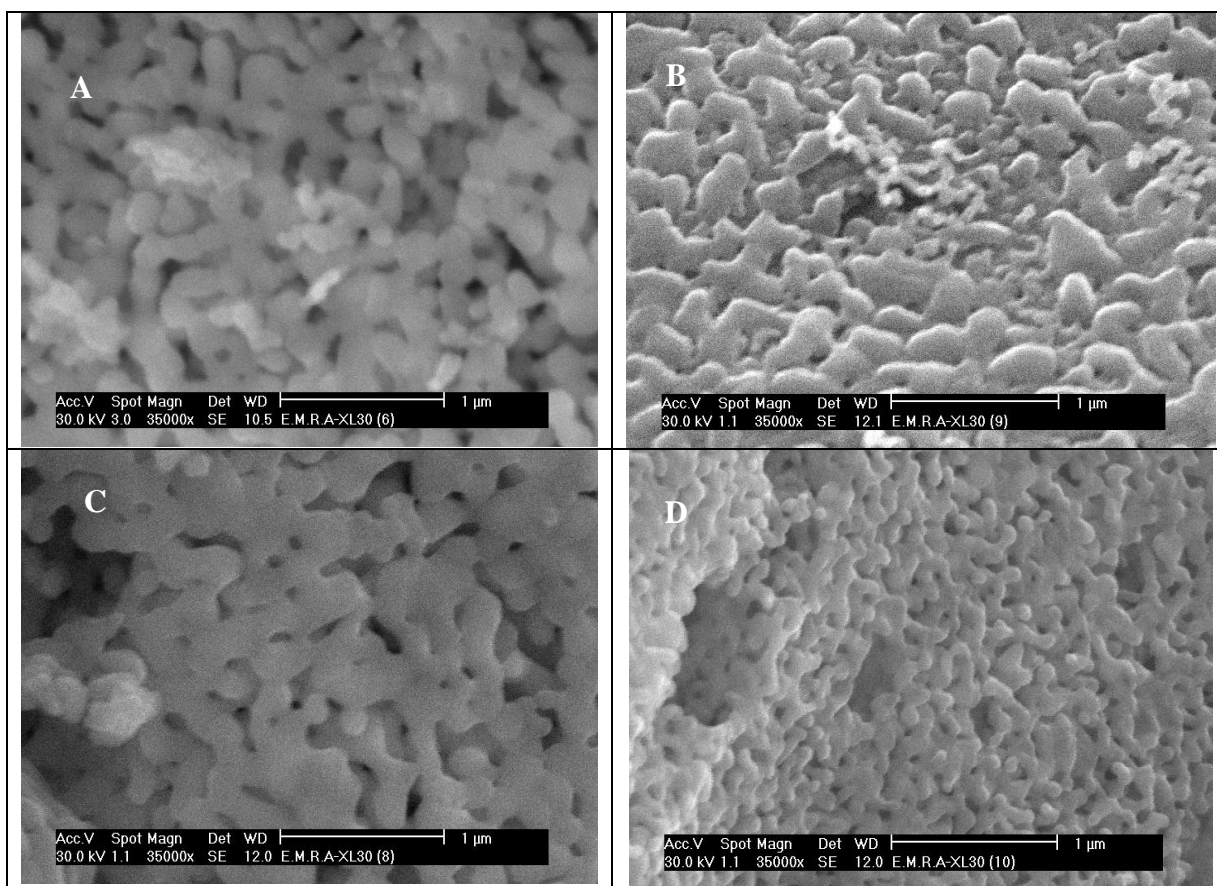


Figure 2. SEM micrographs of (A) LaFeO₃, (B) NdFeO₃, (C) SmFeO₃ and (D) GdFeO₃ prepared by the microwave-assistant citrate method at 720 W for 30 min, with a magnification of 35,000 times.

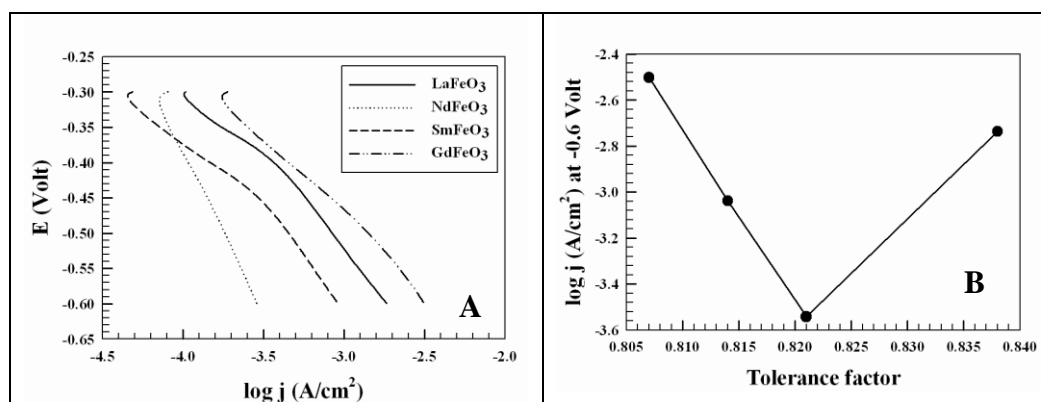


Figure 3. (A) Linear Tafel polarization curves for the HER recorded on CPEs modified with 10% (w/w%) (—) LaFeO₃, (...) NdFeO₃, (---) SmFeO₃ and (-.-.-) GdFeO₃ prepared by the microwave-assistant citrate method at 720 W for 30 min in 0.1M H₂SO₄, scan rate=1 mV.s⁻¹. And (B) the dependence of the HER rate on the tolerance factor.

The electrocatalytic activity of the prepared perovskites, LnFeO_3 ($\text{Ln} = \text{La}, \text{Nd}, \text{Sm}$ and Gd) toward HER was investigated by Tafel linear polarization measurements. Figure 3A shows a set of Tafel curves recorded in 0.1 M H_2SO_4 in the potential region of hydrogen evolution for CPEs modified with 10% (w/w%) LnFeO_3 ($\text{Ln} = \text{La}, \text{Nd}, \text{Sm}$ and Gd) prepared by the microwave assistant-citrate method at an operating microwave power of 720 W and a microwave irradiation time of 30 min, Figure 3B showed the dependence of the cathodic current on the tolerance factor.

The order of the electrocatalytic activity was $\text{GdFeO}_3 > \text{LaFeO}_3 > \text{SmFeO}_3 > \text{NdFeO}_3$. In other words, the catalytic activity of LnFeO_3 ($\text{Ln} = \text{La}, \text{Nd}, \text{Sm}$ and Gd) for the HER increased by increasing the tolerance factor, with two exceptions in case of GdFeO_3 and NdFeO_3 . However, these two exceptions (the low unexpected catalytic activity for NdFeO_3 and the high unexpected catalytic activity for GdFeO_3) would be cancelled as shown later in the activation energy calculations section. The existence of two Tafel regions (change in Tafel slope) has already been reported in literature [15] for similar HER electrocatalytic materials, and a number of explanations have been given, a change in HER mechanism has been suggested as one possible explanation, which can be attributed to the depletion of the d-electron density at the Fermi level of the perovskite by adsorbed hydrogen [16] which remained partially uncompensated at lower overpotentials. Mass-transport limitations through narrow pores on the catalyst surface [17] or a decrease in the active surface area [18-20] have also been suggested as possible reason for the observed diffusion-like shape of the Tafel curves. By considering the Tafelian region, the calculated values of Tafel slope, exchange current density, and transfer coefficient for the prepared perovskites were calculated and listed in Table 2.

Table 2. HER kinetic parameters obtained by analysis of Linear Tafel polarization curves, together with the tolerance factors for LnFeO_3 ($\text{Ln} = \text{La}, \text{Nd}, \text{Sm}$ and Gd) prepared by the microwave-assistant citrate method at 720 W for 30 min.

	Tolerance factor	b/ mV.dec^{-1}	j_0 / $\mu\text{A.cm}^{-2}$	α	j / $\mu\text{A.cm}^{-2}$ at -400 mV	η / mV at 0.5 mA/cm^{-2}
LaFeO_3	0.838	232.4	-5.86	0.25	-367.37	-394
NdFeO_3	0.821	238.8	-14.59	0.26	-107.82	-595
SmFeO_3	0.814	209.1	-1.68	0.29	-147.23	-446
GdFeO_3	0.807	216.9	-6.53	0.28	-451.86	-360

According to the general HER mechanism in acidic media [21-23], these Tafel slope values indicated that the Volmer reaction step i.e. adsorption of hydrogen on the catalyst was the rate-determining step. It could also be noticed that the Tafel slope and transfer coefficient values deviated from the theoretical values $116 \text{ mV decade}^{-1}$ and 0.5 respectively [21-23]. This phenomenon has already been reported in the literature [24] and has been explained as a characteristic feature for oxide catalysts. By considering the current density values, measured at a fixed overpotential of -400mV and the overpotential values, measured at current density of 0.5 mA.cm^{-2} , which were presented in Table 2, it can be concluded that the order catalytic activity was also $\text{GdFeO}_3 > \text{LaFeO}_3 > \text{SmFeO}_3 > \text{NdFeO}_3$.

However, by considering the exchange current density values, presented in Table 2, the order of the electrocatalytic activity was $\text{NdFeO}_3 > \text{GdFeO}_3 > \text{LaFeO}_3 > \text{SmFeO}_3$. The data showed that NdFeO_3 has the highest catalytic activity for the HER among the prepared series at equilibrium. This result will be confirmed later by the activation energy calculations which depend on the equilibrium state (the exchange current density values).

3.3. Order of reaction with respect to H^+

The order of the reaction with respect to H^+ was determined at constant ionic strength of the solution by varying the H_2SO_4 concentration keeping the ionic strength constant with Na_2SO_4 . Only one DC polarization measurement was taken at each H_2SO_4 concentration by the same procedure mentioned in the experimental section. Figure 4A shows a set of Tafel curves recorded in x M H_2SO_4 ($x = 0.05, 0.1, 0.2, 0.3, 0.4,$ and 0.5M) in the potential region of hydrogen evolution for CPE modified with 10% (w/w%) NdFeO_3 , the same data for the other prepared perovskites are not displayed. Figure 4B represents the dependence of the cathodic current of HER on the H^+ ion concentration. The reaction order values of LnFeO_3 ($\text{Ln} = \text{La}, \text{Nd}, \text{Sm}$ and Gd) were 0.37, 0.72, 0.41 and 0.72 respectively. The fractional reaction order was expected for HER catalyzed by oxide catalysts [24].

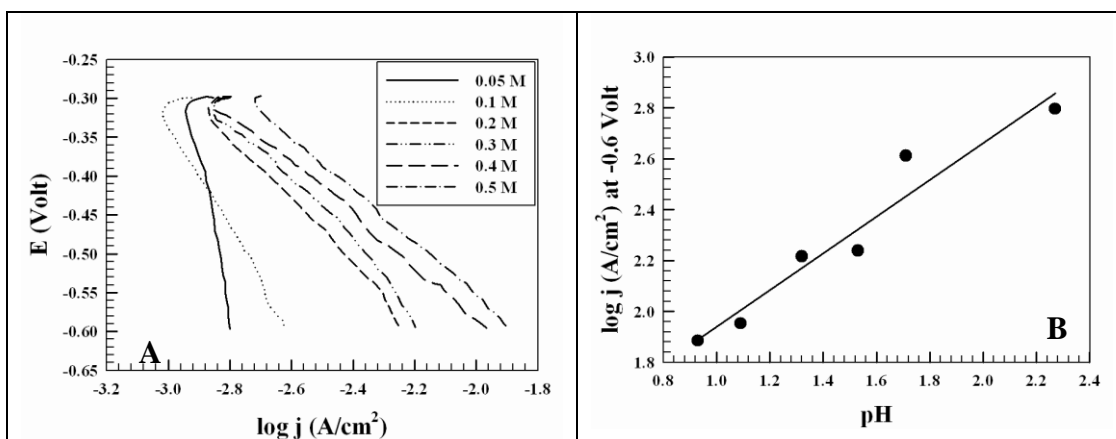


Figure 4. (A) Linear Tafel polarization curves for the HER recorded on CPE modified with 10% (w/w%) NdFeO_3 prepared by the microwave-assistant citrate method at 720 W for 30 min in x M H_2SO_4 ; $x =$ (—) 0.05, (...) 0.1, (---) 0.2, (-.-.-) 0.3, (- -) 0.4 and (-.-.-) 0.5 M at room temperature, scan rate=1 $\text{mV}\cdot\text{s}^{-1}$. (B) typical plot of $\log j$ (A/cm^2) at -0.6 Volt (Saturated Ag/AgCl) vs. pH for the determination of the reaction order for NdFeO_3 .

3.4. Activation energy

In order to evaluate the temperature effect on the kinetics of the HER for the prepared catalysts, DC linear polarization (Tafel) measurements were done for a wide temperature range, from 298K to 338K. Figure 5A shows a set of Tafel curves recorded on CPE modified with 10% (w/w%) NdFeO_3 at

various temperatures. Figure 5B demonstrated that this increase was linear in a semi-logarithmic plot, the Arrhenius equation.

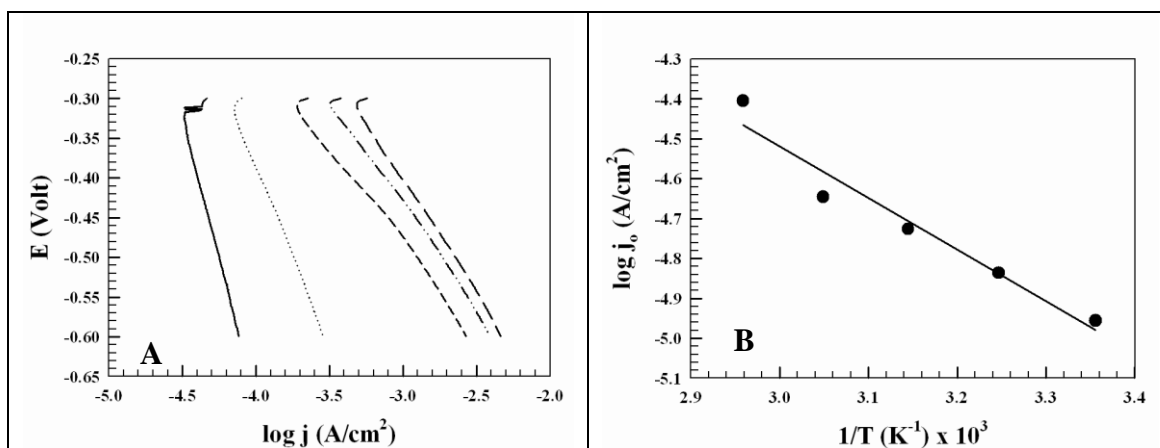


Figure 5. (A) Linear Tafel polarization curves for the HER recorded on CPE modified with 10% (w/w%) NdFeO₃ prepared by the microwave-assistant citrate method at 720 W for 30 min in 0.1 M H₂SO₄ at various temperatures; (—) 298, (...) 308, (---) 318, (-.-.-) 328 and (— —) 338 K; scan rate=1 mV.s⁻¹. (B) Arrhenius plot for the determination of activation energy values for NdFeO₃.

The activation energy values for LnFeO₃ (Ln = La, Nd, Sm and Gd) were 41.15, 24.68, 57.89 and 81.37 kJ mol⁻¹, respectively. Thus, the order of the electrocatalytic activity for HER was NdFeO₃ > LaFeO₃ > SmFeO₃ > GdFeO₃. This trend agreed somehow with that based on the exchange current density values, which was NdFeO₃ > GdFeO₃ > LaFeO₃ > SmFeO₃. The difference between the two trends can be explained on the basis that the catalytic activity of GdFeO₃ was decreased by rising temperature, which was expected since GdFeO₃ had the smallest tolerance factor and hence the lowest thermal stability. Thus, based on the order of the catalytic activity obtained from the activation energy calculations, the catalytic activity of LnFeO₃ (Ln = La, Nd, Sm and Gd) for the HER increased by increasing the tolerance factor. However, the tolerance factor can not be taken as the only measure for the electrocatalytic activity (NdFeO₃ was more active catalyst than LaFeO₃, although it has a smaller value of tolerance factor), more effective factor for elucidating this order of activity is the nature of the A cation. The difference in chemical composition of LnFeO₃ (Ln = La, Nd, Sm and Gd), caused by different A cations, led to differences in structural and catalytic properties.

The Fe–O bond strength should be considered as relevant when a correlation is related to some chemical properties, such as catalytic performance and structural ones of the AFeO₃ perovskites [25]. The redox properties of the materials and their catalytic behavior may be linked, for instance, to their structural characteristics. If lattice oxygen, in addition to the surface one, of the perovskite catalyst is involved in oxidation reactions, less reducible materials obtained leading to less active catalysts i.e. (having stronger Fe–O bonds and oxygen more strongly bonded). The average Fe–O distances may be estimated from the cell size of the idealized cubic lattice [26]. By taking into account the b values, calculated from XRD data (5.579, 5.587, 5.574 and 5.565 Å for LaFeO₃, NdFeO₃, SmFeO₃ and

GdFeO₃, respectively), the corresponding estimated inter-ionic distances (Fe–O = 1/4 b) were 1.395, 1.397, 1.393 and 1.391 Å for LaFeO₃, NdFeO₃, SmFeO₃ and GdFeO₃, respectively. Thus the bond strength order was GdFeO₃ > SmFeO₃ > LaFeO₃ > NdFeO₃ and the catalytic activity order was NdFeO₃ > LaFeO₃ > SmFeO₃ > GdFeO₃. The last order agreed well with that concluded from the activation energy calculations. The estimated Fe–O distances were much shorter than the value (2.045 Å). It was expected on the basis of the sum of the ionic radii ($r_{\text{Fe}^{3+}} = 0.645\text{Å}$ for high spin electron configuration in octahedral coordination, $r_{\text{O}^{2-}} = 1.40\text{Å}$ [27]). This feature may suggest that a certain degree of covalence was present in the Fe–O bonds, whose nature may also depend on the type of the partner A rare-earth ion.

3.5. Electrochemical impedance spectroscopy

Figures 6A and 6B show examples of EIS spectra recorded on CPE modified with 10% (w/w%) NdFeO₃ at overpotential of -0.1 V. The data were presented in the form of both Nyquist and Bode plots.

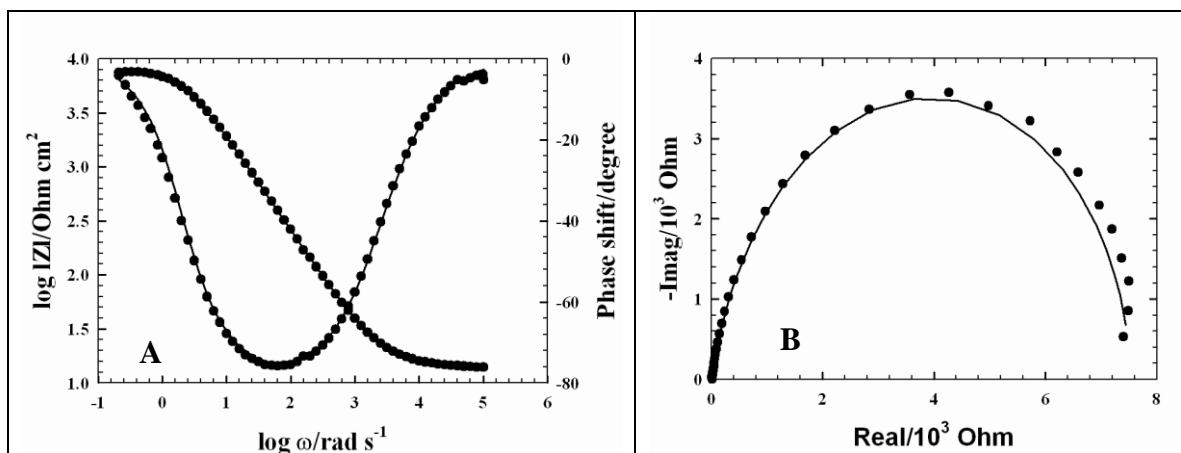


Figure 6. (A) Bode and (B) Nyquist plots showing An EIS response of CPE modified with 10% (w/w%) NdFeO₃ prepared by the microwave-assistant citrate method at 720 W for 30 min in 0.1M H₂SO₄ at ovepotential -0.1V, symbols are experimental and solid lines are modeled data.

The EIS spectra revealed the presence of two time constants. In order to derive a physical picture of the electrode/electrolyte interface and the processes occurring at the electrode surface, experimental EIS data were modeled using non-linear least-squares fit analysis (NLLS) software and electrical equivalent circuit. Figures 6A and 6B show that a very good agreement between the experimental (symbols) and simulated (lines) data was obtained when the equivalent circuit shown in Figure 7 was used to describe the EIS response of the investigated catalysts.

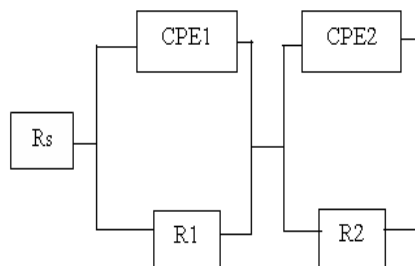


Figure 7. Electrical equivalent circuit used to explain the EIS response of the HER.

This model has been used to describe the response of the HER on porous electrodes [22, 28, 29]. It reflects the response of a HER system characterized by two time constants, only one of them (CPE1) is related to the kinetics of the HER. This time constant changes with overpotential. The second time constant (CPE2) is related to the porosity of the electrode surface, and does not change with overpotential. The dependence of each electrical equivalent circuit parameter on applied overpotential was investigated. Figure 8 shows a set of EIS spectra recorded on CPE modified with 10% (w/w%) NdFeO_3 at various overpotentials.

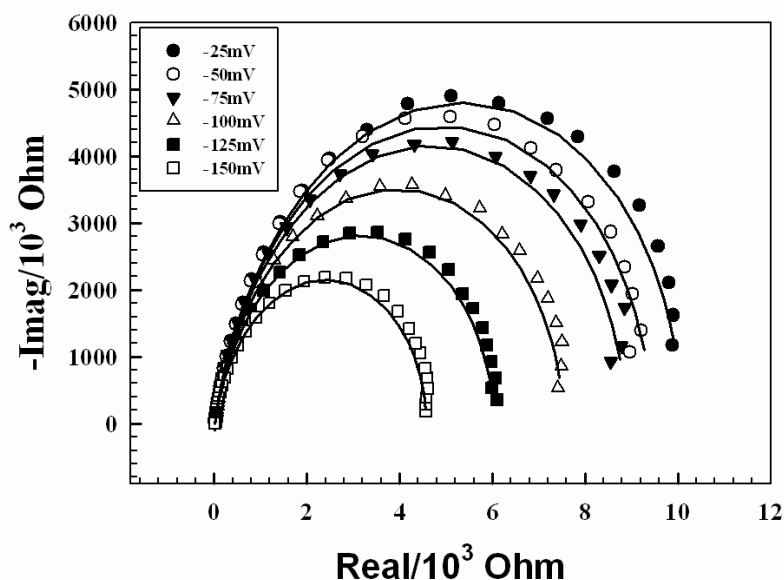


Figure 8. Nyquist plots showing An EIS response of CPE modified with 10% (w/w%) NdFeO_3 prepared by the microwave-assistant citrate method at 720 W for 30 min in 0.1M H_2SO_4 at various overpotentials, (\bullet) -50, (\circ) -75, (\blacktriangledown) -100, (Δ) -125 and (\blacksquare) -150 mV, symbols are experimental and solid lines are modeled data.

Tables 3a, 3b, 3c and 3d show the electrical equivalent circuit parameters calculated from NLLS analysis for LnFeO_3 ($\text{Ln} = \text{La}, \text{Nd}, \text{Sm}$ and Gd) prepared by microwave assistant-citrate method, respectively.

Table 3. The electrical equivalent circuit parameters calculated from the NLLS analysis for (a) LaFeO₃, (b) SmFeO₃, (c) NdFeO₃ and (d) GdFeO₃ prepared by the microwave-assistant citrate method at 720 W for 30 min.

(a)

η/V	$R_s/\Omega\text{ cm}^2$	$CPE1/F\text{ cm}^{-2}$	m	$R1/\Omega\text{ cm}^2$	$CPE2/F\text{ cm}^{-2}$	n	$R2/\Omega\text{ cm}^2$
-0.025	8.52	136466.49	0.92	81009.07	25.99	0.29	10.09
-0.050	6.79	147493.98	0.93	58160.48	25.92	0.06	42.80
-0.075	7.36	154830.11	0.93	47829.09	28.04	0.07	35.40
-0.100	8.13	157187.92	0.93	35938.87	31.39	0.08	28.33
-0.125	3.92	161511.03	0.93	30146.87	26.41	0.05	18.94
-0.150	0.14	163595.43	0.94	20663.91	23.78	0.03	9.74

(b)

η/V	$R_s/\Omega\text{ cm}^2$	$CPE1/F\text{ cm}^{-2}$	m	$R1/\Omega\text{ cm}^2$	$CPE2/F\text{ cm}^{-2}$	n	$R2/\Omega\text{ cm}^2$
-0.025	1.82	147558.73	0.92	33841.07	236422300.80	0.90	2314.94
-0.050	2.73	158146.39	0.93	24755.70	221821010.00	0.89	2250.93
-0.075	1.07	162384.76	0.93	19124.49	232043604.50	0.89	2205.92
-0.100	2.69	165082.95	0.94	13762.34	247836743.10	0.85	2216.44
-0.125	6.98	168172.17	0.94	9931.23	213704292.80	0.93	1705.39
-0.150	1.00	175144.04	0.96	8067.08	204843442.30	0.93	1697.72

(c)

η/V	$R_s/\Omega\text{ cm}^2$	$CPE1/F\text{ cm}^{-2}$	m	$R1/\Omega\text{ cm}^2$	$CPE2/F\text{ cm}^{-2}$	n	$R2/\Omega\text{ cm}^2$
-0.025	14.39	71709.62	1.02	7599.18	22669.09	0.79	2824.92
-0.050	14.33	75683.89	1.04	7392.42	21646.01	0.81	2670.29
-0.075	14.19	77711.21	1.02	6685.82	28363.76	0.81	2192.58
-0.100	14.03	82127.23	1.01	5844.28	25154.72	0.80	1679.50
-0.125	13.90	86313.84	1.01	4726.87	23663.73	0.80	1305.79

-0.150	13.79	90399.16	1.02	3500.72	25365.71	0.80	1066.66
--------	-------	----------	------	---------	----------	------	---------

(d)

η/V	$R_s/\Omega\text{ cm}^2$	$CPE1/F\text{ cm}^{-2}$	m	$R1/\Omega\text{ cm}^2$	$CPE2/F\text{ cm}^{-2}$	n	$R2/\Omega\text{ cm}^2$
-0.025	14.33	155035.41	1.04	14718.75	64315.29	0.83	2914.82
-0.050	14.24	165816.22	1.07	11536.40	67166.17	0.86	3830.57
-0.075	14.04	192242.17	1.04	10155.85	64506.76	0.83	2920.93
-0.100	13.84	193619.22	1.11	6271.85	71849.48	0.86	2442.07
-0.125	13.70	228262.59	1.13	4395.59	68484.81	0.88	2320.05
-0.150	13.62	253856.83	1.06	3698.59	66157.72	0.86	1610.33

With an increase in overpotential, CPE1 increased and R1 decreased. It can be concluded that the (CPE1-R1) is related to the HER charge-transfer kinetics, namely to the response of double layer capacitance characterized by CPE1 and HER charge transfer resistance characterized by R1. In contrary to the behavior of CPE1, the value of CPE2 was shown to be relatively constant. At the same time, the value of R2 decreased. This is a typical behavior related to the porosity of the electrode surface.

3.6. The effect of the partial substitution at the A-site, $La_{1-y}Sm_yFeO_3$, on the catalytic activity

A series of perovskite catalysts, $La_{1-y}Sm_yFeO_3$ ($y = 0.25, 0.5$ and 0.75) was prepared by microwave assistant-citrate method at an operating microwave power of 720 W and a microwave irradiation time of 30 min. Figures 9A, 9B and 9C show the XRD patterns of $La_{1-y}Sm_yFeO_3$ ($y = 0.25, 0.5$ and 0.75) prepared by microwave assistant-citrate method respectively, the results showed that only binary perovskites were formed. For Sm-doped $LaFeO_3$, a single phase of $LaFeO_3$ or $SmFeO_3$ was formed in case of small or high doping fraction, respectively. While in case of $y = 0.5$, a mixture of both $LaFeO_3$ and $SmFeO_3$ was obtained.

The morphology of the prepared perovskites was studied by SEM. Figures 10A, 10B and 10C show the SEM images of $La_{1-y}Sm_yFeO_3$ ($y = 0.25, 0.5$ and 0.75) prepared by microwave assistant-citrate method, respectively.

Figure 10A shows the SEM image for $La_{0.75}Sm_{0.25}FeO_3$, the surface was porous as that of $LaFeO_3$. Figure 10C shows the SEM image for $La_{0.25}Sm_{0.75}FeO_3$, which was compact as that of $SmFeO_3$. While Figure 10B shows the SEM image for $La_{0.5}Sm_{0.5}FeO_3$, the surface has a porous region and other compact region, which suggested the presence of two different phases.

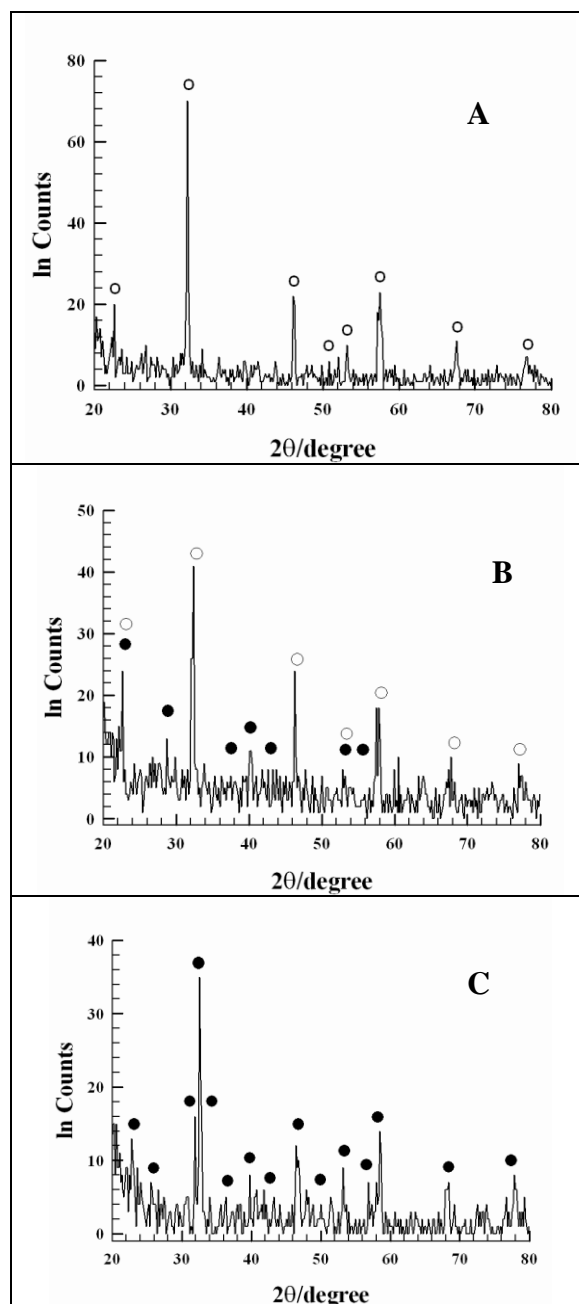


Figure 9. XRD patterns of (A) $\text{La}_{0.75}\text{Sm}_{0.25}\text{FeO}_3$, (B) $\text{La}_{0.5}\text{Sm}_{0.5}\text{FeO}_3$ and (C) $\text{La}_{0.25}\text{Sm}_{0.75}\text{FeO}_3$ prepared by the microwave assistant-citrate method at 720 W for 30 min, (\circ LaFeO_3 and \bullet SmFeO_3).

The prepared perovskites were tested as catalysts for the HER. Figure 11 shows the dependence of the cathodic current on the fraction of Sm in Sm-doped LaFeO_3 .

The order of the electrocatalytic activity was $\text{La}_{0.75}\text{Sm}_{0.25}\text{FeO}_3 > \text{La}_{0.5}\text{Sm}_{0.5}\text{FeO}_3 > \text{La}_{0.25}\text{Sm}_{0.75}\text{FeO}_3 > \text{LaFeO}_3 > \text{SmFeO}_3$. From this order it can be concluded that the catalytic activity of ternary perovskites was much higher than that of binary ones. Among ternary perovskites, the catalytic activity decreased by increasing the fraction of doped-Sm. This was expected when La in the

A-site was doped by less active Sm (where, activation energies of LaFeO_3 and SmFeO_3 were 41.15 and 57.89 $\text{kJ}\cdot\text{mol}^{-1}$, respectively).

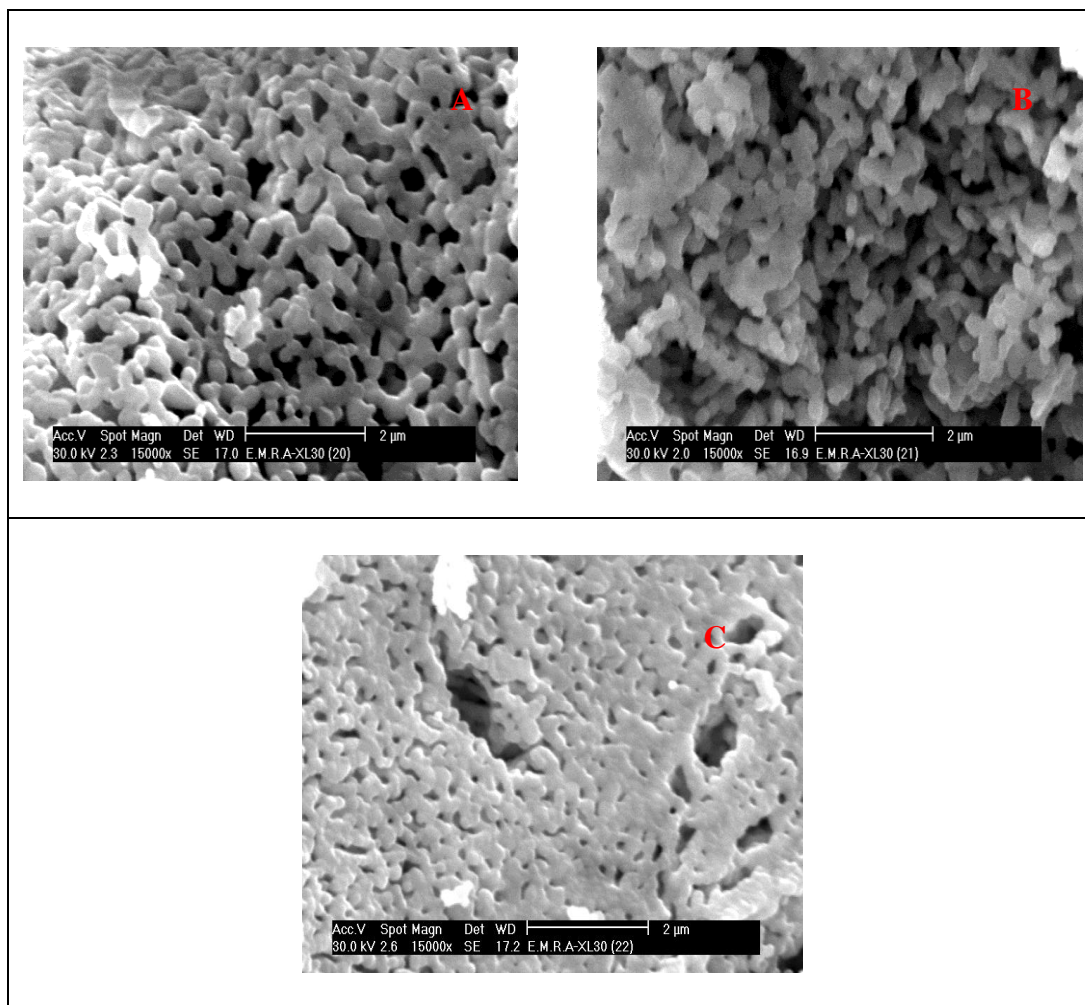


Figure 10. SEM micrographs of (A) $\text{La}_{0.75}\text{Sm}_{0.25}\text{FeO}_3$, (B) $\text{La}_{0.5}\text{Sm}_{0.5}\text{FeO}_3$ and (C) $\text{La}_{0.25}\text{Sm}_{0.75}\text{FeO}_3$ prepared by the microwave-assistant citrate method at 720 W for 30 min, with a magnification of 15,000 times.

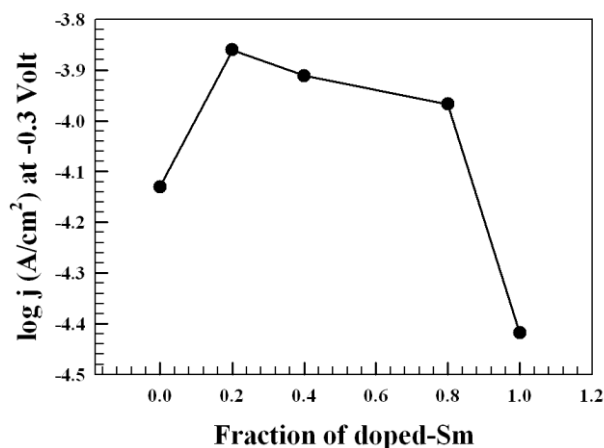


Figure 11. A typical plot of $\log j \text{ (A/cm}^2\text{) at -0.3 Volt}$ (Saturated Ag/AgCl) vs. the fraction of Sm-doped.

4. CONCLUSION

For LnFeO_3 ($\text{Ln} = \text{La}, \text{Nd}, \text{Sm}$ and Gd), the order catalytic activity for HER based on the values of exchange current density was $\text{NdFeO}_3 > \text{GdFeO}_3 > \text{LaFeO}_3 > \text{SmFeO}_3$ and the order of the electrocatalytic activity based on activation energies calculations was $\text{NdFeO}_3 > \text{LaFeO}_3 > \text{SmFeO}_3 > \text{GdFeO}_3$. The difference between the two trends can be explained on the basis that the catalytic activity of GdFeO_3 was decreased by rising temperature. Which was expected since GdFeO_3 had the smallest tolerance factor and hence the lowest thermal stability. However, the tolerance factor can not be taken as the only measure for the electrocatalytic activity (NdFeO_3 was more active catalyst than LaFeO_3 , although it has a smaller value of tolerance factor), more effective factor for elucidating this order of activity is the nature of the A cation. The catalytic activity order based on the Fe-O bond strength, which affected by the A-type metal ion, was $\text{NdFeO}_3 > \text{LaFeO}_3 > \text{SmFeO}_3 > \text{GdFeO}_3$. This agreed well with that concluded from the activation energy calculations.

For Sm-doped LaFeO_3 , The order of the electrocatalytic activity was $\text{La}_{0.75}\text{Sm}_{0.25}\text{FeO}_3 > \text{La}_{0.5}\text{Sm}_{0.5}\text{FeO}_3 > \text{La}_{0.25}\text{Sm}_{0.75}\text{FeO}_3 > \text{LaFeO}_3 > \text{SmFeO}_3$. Thus, the catalytic activity of ternary perovskites was higher than that of binary ones. Among ternary perovskites, the catalytic activity decreased by increasing the fraction of doped-Sm. This was expected when La in the A-site was doped by less active Sm.

References

1. M. Z. Jacobson, W. G. Colella and D. M. Golden, *Science*, 308 (2005) 1901.
2. C. Hamann, A. Hamnett, W. Vielstich, *Electrochemistry*, Wiley-VCH, Weinheim, (1998).
3. CRC, *Handbook of Chemistry and Physics*, CRC Press, New York, (1996).
4. E. Navarro-Flores and S. Omanovic, *J. Mol. Catal. A: Chem.*, 242 (2005) 182.
5. M.P. Selvam and K.J. Rao, *Adv. Mater.*, 12 (2000) 1621.
6. K.E. Gibbons, M.O. Jones, I. Gameson, P.P. Edwards, Y. Miyazaki, N.C. Hyatt, S.J. Blundell, A.I. Mihut, A. Porch, *Chem. Comm.*, 2 (2000) 159.
7. M. Panneerselvam and K.J. Rao, *J. Mater. Chem.*, 13 (2003) 596.
8. H. Yan, X. Huang, L. Zhonghua, H. Huang, R. Xue and L. Chen, *J. Pow. Sources*, 68 (1997) 530.
9. R. Ran, D. Weng, X. Wu, J. Fan and L. Qing, *Catal. Today*, 126 (2007) 394.
10. J. Mawdsley, M. Ferrandon, C. Rossignol, J. Ralph, L. Miller, J. Kopasz, T. Krause, *Hydrogen, Fuel Cells and Infrastructure Technologies*, Merit Review, Berkeley, CA, (2003).
11. A. Galal, S.A. Darwish, N.F. Atta, S.M. Ali and A.A. Abd El Fatah, *Appl. Catal. A: Gen.*, 378 (2010) 151.
12. A. Galal, N.F. Atta and S.M. Ali, *Appl. Catal. A: Gen.*, 409-410 (2011) 202.
13. A. Galal, N.F. Atta and S.M. Ali, *Electrochim. Acta*, 56 (2011) 5722.
14. B.D. Cullity, *Elements of X-ray diffraction*, 2nd ed., Wiley pub. company, U.S.A, (1978).
15. A. Damian and S. Omanovic, *J. Pow. Sources*, 158 (2006) 464.
16. K.R. Christmann, In: Z. Poal, P.G. Menon (Eds), *Hydrogen Effects in Catalysis*, Marcel Dekker, (1988).
17. J. G. Highfield, K. Oguro and B. Grushko, *Electrochim. Acta*, 47 (2001) 465.
18. A. Rami and A. Lasia, *J. Appl. Electrochem.*, 22 (1992) 376.
19. N. Krstajic and S. Trasatti, *J. Appl. Electrochem.*, 28 (1998) 1291.
20. C. A. Marozzi and A. C. Chialvo, *Electrochim. Acta*, 46 (2001) 861.

21. Southampton Electrochemistry group, *Instrumental Methods in Electrochemistry*, Wiley, New York, (1985).
22. B. Borresen, G. Hagen and R. Tunold, *Electrochim. Acta*, 47(2002) 1819.
23. E. Ndzebet and O. Savadogo, *Inter. J. Hydrogen Energy*, 20 (1995) 635.
24. E. Fachinotti, E. Guerrini, A.C. Tavares and S. Trasatti, *J. Electroanal. Chem.*, 600 (2007) 103.
25. P. Porta, S. Cimino, S. De Rossi, M. Faticanti, G. Minelli and I. Pettiti, *Mater. Chem. Phys.*, 71 (2001) 165.
26. S. Geller and E.A. Wood, *Acta Crystal.*, 9 (1956) 563.
27. R.D. Shannon, *Acta Crystal.*, 32 (1976) 751.
28. B. Losiewicz, A. Budniok, E. Rówiniski, E. Lagiewka and A. Lasia, *Inter. J. Hydrogen Energy*, 29 (2004)145.
29. L. Birry and A. Lasia, *J. Appl. Electrochem.*, 34 (2004) 735.